International Journal of Heat and Mass Transfer 52 (2009) 2119–2131

Contents lists available at ScienceDirect

International Journal of Heat and Mass Transfer

journal homepage: www.elsevier.com/locate/ijhmt

Flow visualizations and heat transfer measurements for a rotating pin-fin heat sink with a circular impinging jet

Tzer-Ming Jeng [a,*], Sheng-Chung Tzeng [b], Hong-Ru Liao [b]

[a] Department of Mechanical Engineering, Air Force Institute of Technology, GangShan 820, Taiwan, ROC
[b] Department of Mechanical Engineering, Chienkuo Technology University, ChanGhua 500, Taiwan, ROC

ARTICLE INFO

Article history:
Received 30 May 2008
Received in revised form 20 October 2008
Available online 26 December 2008

Keywords:
Heat transfer
Jet impingement
Rotating heat sink
Smoke visualization

ABSTRACT

This work experimentally investigated the fluid flow and heat transfer behaviors of jet impingement onto the rotating heat sink. Air was used as impinging coolant, while the square heat sinks with uniformly in-line arranged 5×5 and 9×9 pin-fins were employed. The side length (L) of the heat sink equaled 60 mm and was fixed. Variable parameters were the relative length of the heat sink (L/d = 2.222 and 4.615), the relative distance of nozzle-to-fin tip (C/d = 0–11), the jet Reynolds number (Re = 5019–25,096) and the rotational Reynolds number (Re_r = 0–8114). Both flow characteristics of stationary and rotating systems were illustrated by the smoke visualization. Besides, the results of heat transfer indicate that, for a stationary system with a given air flow rate, there was a larger average Nusselt number (Nu_0) for the 9×9 pin-fin heat sink with L/d = 4.615 and C/d = 11. For a rotating system, a bigger Re_r meant a more obvious heat transfer enhancement (Nu_Ω/Nu_0) in the case of smaller Re, but Nu_Ω/Nu_0 decreased with increasing Re. In this work, Nu_Ω/Nu_0 in L/d = 2.222 is higher than in L/d = 4.615; among the systems in L/d = 2.222, bigger Nu_Ω/Nu_0 exists in the case of C/d = 9–11, but among the systems in L/d = 4.615, bigger Nu_Ω/Nu_0 exists in the case of C/d = 1–3. Finally, according to the base of $Nu_\Omega/Nu_0 \geqslant 1.1$, the criterion of the substantial rotation was suggested to be $Re_r/Re \geqslant 1.154$.

1. Introduction

Jet impingement can provide large localized cooling for many industrial applications, such as annealing metals, tempering glass, drying paper and textiles, and cooling of gas turbine blades and electronics equipment. Jambunathan et al. [1] reviewed the heat transfer data for single circular jet impingement and summarized four flow zones commonly appeared at such systems: (1) initial mixing zone, (2) established jet zone, (3) impingement zone, and (4) wall jet zone. In an impinging-cooling system, the fluid flow strongly influences the heat transfer. Consequently, the parameters that may affect heat transfer include: the jet Reynolds number (Re), the Prandtl number (Pr), the dimensionless distance of nozzle-to-plate (H/d), the dimensionless displacement from the stagnation point (x/d), the nozzle geometry, the flow confinement, the velocity profile at the nozzle exit, the turbulence intensity of jet flow, and etc.

Many studies had considered the heat transfer of the impinging jet onto a heated and stationary plate [1–6]. To further improve the cooling performance of jet impingement, the heat sink with extended surface is mounted onto the heated plate. Besides the increase of the heat dissipation area, the turbulence due to the separation and reattachment of fluid flow across fins also facilitates heat transfer between fluid and fins. The relevant researches are described below. Sathe et al. [7] presented the three-dimensional numerical simulations of the impinging jet onto the pin-fin heat sink. The heat sink used in their analysis, had a $59 \times 59 \times 2$ mm ceramic base, over which a total of 256 square pin-fins were arranged in a regular in-line pattern. Each pin-fin was 25 mm tall and had a square cross section of 2×2 mm. The cooling air entered the pin-fin heat sink through a nozzle situated 3 mm above the pin-fin tips at the center of the heat sink. Almost 64 pin-fins were directly impinged by the air jet in their tests. They reported that the part of the heated base directly below the nozzle was well cooled with the temperatures gradually increasing from the center towards the corner. Sparrow and his colleagues [8–10] experimentally and theoretically explored the heat transfer from the in-line cylindrical pin-fins with an oncoming longitudinal flow which turned 90 deg to exit the pin-fin array. The area of the fluid inlet was as large as the pin-fin array. The fin geometries (such as the relative fin height and the relative inter-fin spacing), Reynolds number, and the fluid inlet and exit geometries (such as with/without the inlet shroud and the extended base plate) were varied. They found that pin-fins situated adjacent to the edges of the array had higher heat transfer coefficient than those situated in the interior of the array. Additionally, they demonstrated that partial shrouding of the inlet could give rise to nearly uniform per-fin heat

* Corresponding author. Tel.: +886 7 6256040; fax: +886 4 7357193.
E-mail addresses: tm.jeng@msa.hinet.net, t_m_jeng@yahoo.com.tw (T.-M. Jeng).

0017-9310/$ - see front matter © 2008 Elsevier Ltd. All rights reserved.
doi:10.1016/j.ijheatmasstransfer.2008.10.028

Nomenclature

A	area of the heated surface (m^2)
C	nozzle-to-fin tip distance (m)
d^*	inner diameter of the vertical tube connecting the nozzle (m)
d	inner diameter of the nozzle (m)
D^*	outer diameter of the nozzle (m)
D	diameter of the circular and heated plate (m)
h	heat transfer coefficient ($W/m^2\,°C$)
H	nozzle-to-plate distance (m)
H_f	height of the pin-fins (m)
I	input current (A)
k	conductivity ($W/m\,°C$)
L	side length of the square heat sink (m)
Nu	average Nusselt number, $Nu = \frac{hL}{k_f} = \frac{q_c L}{(\overline{T}_w - T_j)k_f}$
q_c	convective heat flux (W/m^2)
q_{Loss}	heat loss (W/m^2)
q_t	total input heat flux (W/m^2)
Re	jet Reynolds number, $Re = \frac{\rho_f U_j d}{\mu}$
Re_r	rotational Reynolds number, $Re_r = \frac{\rho_f \pi \Omega L^2}{120\mu}$
t	thickness of the spreader (m)
T	temperature (°C)
V	input voltage (V)
U_j	average fluid velocity at the nozzle exit (m/s)
w	width of the fins (m)

Greek symbols

μ	viscosity of fluid (kg/m/s)
ρ	density (kg/m^3)
θ	nondimensional temperature, $\theta = \frac{T - T_j}{\overline{T}_w - T_j}$
Ω	rotational rate of the heat sink (rpm)

Superscript

–	average

Subscripts

0	stationary state
a	ambient
f	fluid stream
j	jet nozzle
nc	nature convection
w	heated wall
Ω	rotating state

transfer coefficients throughout the array. Furthermore, modifications of the exit geometry affected only the less tightly packed arrays and then only at the outermost row of pin-fins. Hansen and Webb [11] experimentally investigated the heat transfer from finned heat sink with a normally impinging air jet. Four kinds of fin were employed, including the square pin-fin, the pyramidal fin, the concentric fin and the annular fin. As compared to the bare plate, enhancement of the overall heat transfer in their systems was demonstrated by a factor ranging from 1.5 to 4.5. Various nozzle diameters (d, less than the base diameter of the finned heat sink) and nozzle-to-plate distances (H) were used in their tests. They reported that the heat transfer typically decreased with increasing the nozzle diameters or increasing H/d. In addition to, the relationship between the average Nusselt number and the Reynolds number for $H/d = 5$ was proposed. Ledezma et al. [12] provided an experimental, numerical and theoretical study of the heat transfer from the in-line square pin-fins with an oncoming longitudinal flow. They recommended the correlations for the optimal inter-fin spacing to have the maximum thermal conductance in their systems with various fin heights, fin thicknesses, side sizes of the square base plate, Prandtl numbers and oncoming air velocities. Brignoni and Garimella [13] experimentally studied the heat transfer from the circular pin-fin heat sink with a confined air jet impingement. The heat sink had a 20×20 mm base, which was 2.4 mm thick. The fin was 0.9 mm in diameter and 16.4 mm in height. Various nozzle-to-fin tip distances, nozzle diameters and numbers of nozzle were used in their measurements. They found that the nozzle-to-fin tip distance had only modest effect on the heat transfer. Enhancement factors for the heat sink relative to a bare plate were in the range of 2.8–9.7, with the largest value being obtained for the largest single nozzle (12.7 mm diameter). Kondo et al. [14,15] provided a zonal model, based on a series of semi-empirical formula, to determine the thermal resistance and the pressure drop of the finned heat sinks with impingement cooling. Their heat sink configurations were the plate-fin heat sink and the circular pin-fin heat sink. They also performed some typical experiments and flow visualizations to validate the zonal model and used the zonal model to design the optimal finned heat sink. Certainly, due to the leakage flow from the gap between the nozzle and the finned heat sink, their zonal model will not be applicable for a gap more than around 5 mm. Maveety et al. [16–18] experimentally and numerically investigated the heat transfer from the in-line square pin-fin heat sink with a round air jet impingement. The heat sink had a 50.8×50.8 mm base. Two heat sinks with 13×13 and 7×7 pin-fin geometries were used. The diameter of the round nozzle was 6.4 mm. They reported that the optimal performance was achieved when the relative nozzle-to-fin tip distance, C/d, was from 8 to 12 at $Re = 4 \times 10^4$–5×10^4. Additionally, by following the Ledezma et al. [12] method, they showed that the performance of 7×7 pin-fin geometry was superior to that of 13×13 pin-fin geometry. They also illustrated the utility of numerical tests in the design and optimization of such systems. Besides, they demonstrated that the cooling performance gains could be obtained by inserting a deflector plate above the heat sink. Elsheikh and Garimella [19] experimentally investigated the heat transfer enhancement of air jet impingement by using pin-fin heat sinks. In their study, the heat transfer coefficient, for both pinned and unpinned heat sinks, is only modestly dependent on the nozzle-to-target plate spacing (H/d). They also found that the heat transfer coefficient increases as the nozzle diameter decreases at a fixed flow rate. Li and his colleagues [20,21] used infrared thermography to measure the thermal performance of heat sinks with confined impinging air jet. The ratio of heat sink length to nozzle diameter equaled 10 in their tests. They indicated that the thermal resistance decreases with increasing the fin width. Increasing the fin height also decreases the thermal resistance, but the effects are less prominent than those of the fin width. They also reported that an appropriate impinging distance with minimum thermal resistance can be found at a specific Reynolds number, and the optimal impinging distance increases as the Reynolds number increases. Issa and Ortega [22] experimentally measured the pressure drop and heat transfer of a square jet impinging onto the square pin-fin heat sink. Both the sizes of the nozzle and the heat sink base were 25×25 mm. The varied parameters were pin-fin height, pitch and thickness, and the nozzle-to-fin tip distance. They provided a systematically parametric study for such systems. Their conclusions in the aspect of the heat transfer indicated that the overall thermal resistance decreased with increasing pin density

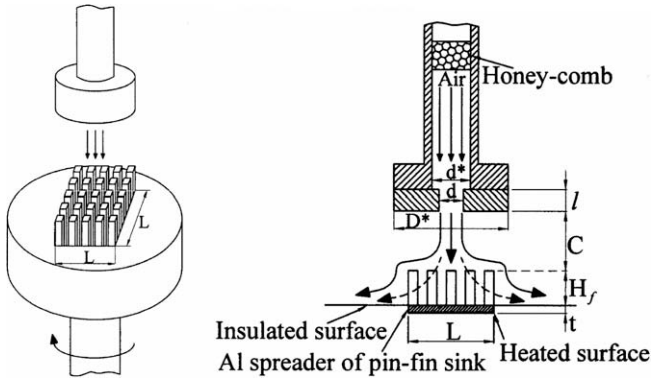

Fig. 1. The physical model of a rotating pin-fin heat sink with a circular impinging jet.

or pin diameter. The effect of pin-fin height on the thermal resistance was weak. Moreover, short pin-fins at low *Re* were most strongly sensitive to variations in tip clearance. Lin et al. [23] experimentally studied the cooling performance of the plate-fin heat sinks with confined slot jet impingement. They proposed a complete composite correlation of steady-state average Nusselt number for mixed convection due to jet impingement and buoyancy.

Impinging-cooling technology is used not only in the cooling of stationary systems, but also in rotating equipment, including rotational trays of chemical vapor deposition (CAD) systems, turbines and electric motors, rotating heat exchangers and high-speed gas bearings. Therefore, various investigations have been performed on the fluid flow and heat transfer characteristics of a rotating disk with an impinging jet [24–27]. The circumferential velocity component induced by rotation promotes convective heat transfer of

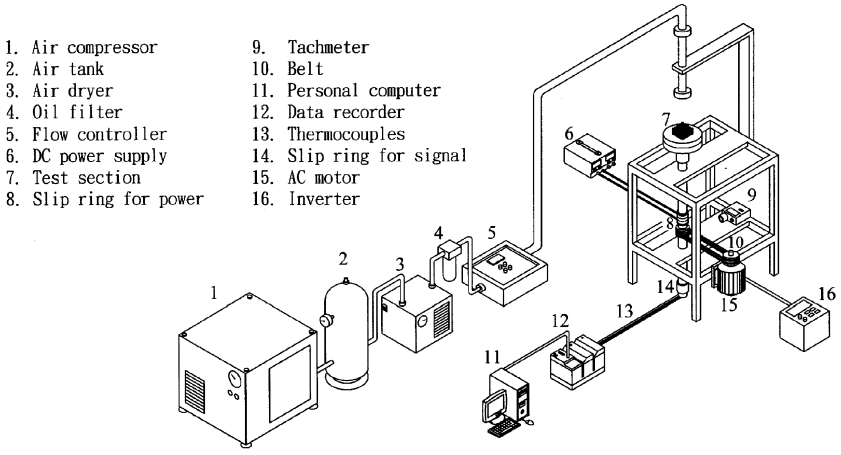

Fig. 2. Experimental apparatus.

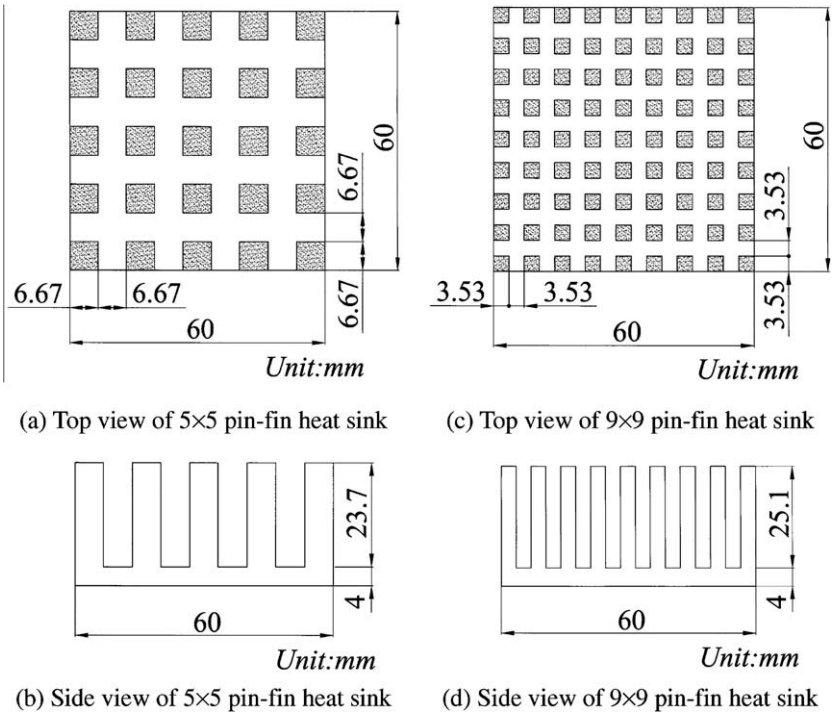

(a) Top view of 5×5 pin-fin heat sink

(c) Top view of 9×9 pin-fin heat sink

(b) Side view of 5×5 pin-fin heat sink

(d) Side view of 9×9 pin-fin heat sink

Fig. 3. The specifications of the heat sinks.

the heated plate. Recently, Jeng et al. [28] experimentally studied heat transfer associated with an impinging air jet onto a rotating Al-foam heat sink. They reported that the rotation considerably enhances the average Nusselt number when the jet Reynolds number (Re) and the relative length of the heat sink (L/d) are small and the relative distance of nozzle-to-fin tip (C/d) is large. The substantial rotations for heat transfer were also suggested for different values of L/d and C/d.

The above studies herein improve our knowledge of heat transfer by impinging jet onto heat sinks. However, few works have addressed the cooling of impinging jet onto rotating heat sinks. This paper aims to explore heat transfer enhancement of jet impingement onto the rotating finned heat sink. Air was used as impinging coolant, while square pin-fin heat sinks with uniformly in-line arrangement were employed. The physical model of a rotating pin-fin heat sink with a circular impinging jet is shown in Fig. 1, wherein variable parameters include: the diameter of jet nozzle, the distance of nozzle-to-fin tip, the amount of flow and the rotational velocity of heat sink. In such systems, the cooling performance of the heat sink is due to two forced convections, i.e. one is resulted from the jet impingement and the other is due to the rotation. It is worthy to investigate the fluid flow and heat transfer characteristics in such systems, with its purpose of improving the cooling design of these systems.

2. Experimental apparatus and test section

The experimental apparatus is shown in Fig. 2. The apparatus comprises four main parts: (1) rotating system; (2) test section; (3) data acquirement system, and (4) air supply system. The rotating system employs a 5 HP AC induction motor to drive the rotating shaft by a belt pulley. An inverter is used to adjust the rotational rate of the motor. The rotational rate of the shaft is measured by a photo-electronic tachometer. The rotating system coupled with the test section is dynamically balanced. The test section is a Bakelite disk sized in 176 mm in diameter and 50 mm in thickness. At the center of Bakelite disk, there is a $60 \times 60 \times 4$ mm square cavity. A film heater, which is heated by a DC power supply through a brush and a power slip ring, is adhered to the bottom surface of the square cavity. Two in-line square pin-fin heat sinks, made of aluminum alloy 6061, are employed in the study. The detailed sizes about the heat sinks are shown in Fig. 3. The heat sink is adhered to the film heater using the highly conductive thermal grease (OMEGABOND 200, k = 1.385 W/m °C). The Bakelite disk has a very low conductivity and can reduce heat loss from the film heater. Nine thermocouples are uniformly embedded in the cavity to measure the temperatures at the bottom of the pin-fin heat sink. All thermocouples cross through the passage in the rotating shaft, and then utilize the data

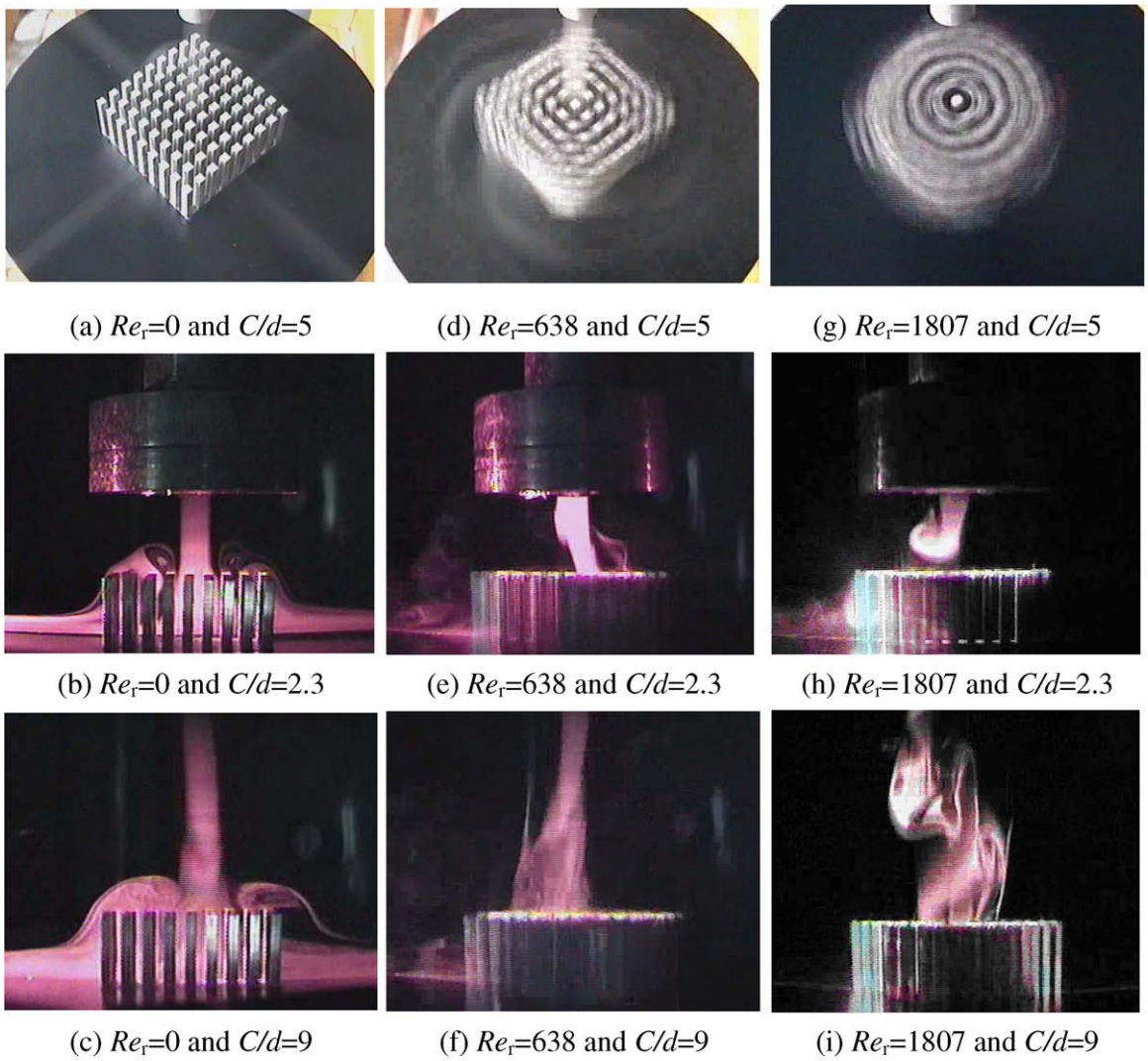

Fig. 4. Flow visualizations in the cases of 9×9 pin-fin heat sink with Re = 1506 and L/d = 4.615.

slip ring to connect to a YOKOGAWA MX-100 data recorder. Another two thermocouples are used to measure the ambient temperature and the jet air temperature. The jet air flow is blown into the air tank by the air compressor. The air initially flows through a dryer and a filter to remove the water, the oil and the particles, and then it enters into a 27-mm diameter vertical pipe with a honey-comb section to straighten the fluid flow, and exits at a circular nozzle, and finally impinges onto the rotating heat sink. The circular nozzle has a length of 13 mm, an external diameter of 84.8 mm, and two inner diameters: 13 mm and 27 mm. The jet air flow rates are determined by a flow controller. The system is assumed to be at the steady-state condition when the temperature variation is within 0.2 °C in 30 min.

3. Data reduction and uncertainty analysis

The measured fluid velocities, rotational rates and temperatures are used to determine the jet Reynolds numbers (Re), the rotational Reynolds number (Re_r) and the average Nusselt numbers (Nu), using

$$Re = \frac{\rho_f U_j d}{\mu} \tag{1}$$

$$Re_r = \frac{\rho_f \pi \Omega L^2}{120\mu} \tag{2}$$

$$Nu = \frac{hL}{k_f} = \frac{q_c L}{(\overline{T_w} - T_j)k_f} \tag{3}$$

where $\overline{T_w}$ is the average temperature at the bottom of the pin-fin heat sink; T_j is the jet air temperature; q_c represents the convective heat flux (i.e. the heat flux removed by the jet flow); U_j is the average air velocity at the nozzle exit; d is the inner diameter of the jet nozzle; Ω is the rotational rate of the pin-fin heat sink, and L is the side length of the square heat sink, respectively. The convective heat flux (q_c) is estimated to be the difference between the total input heat flux (q_t) and the heat loss (q_{Loss}).

$$q_c = q_t - q_{Loss} = V \times I/A - q_{Loss} \tag{4}$$

where A is the area of the heated surface, as well as V and I are the input voltage and current from the DC power supply to the film heater, respectively. The heat loss (q_{Loss}) is measured at the

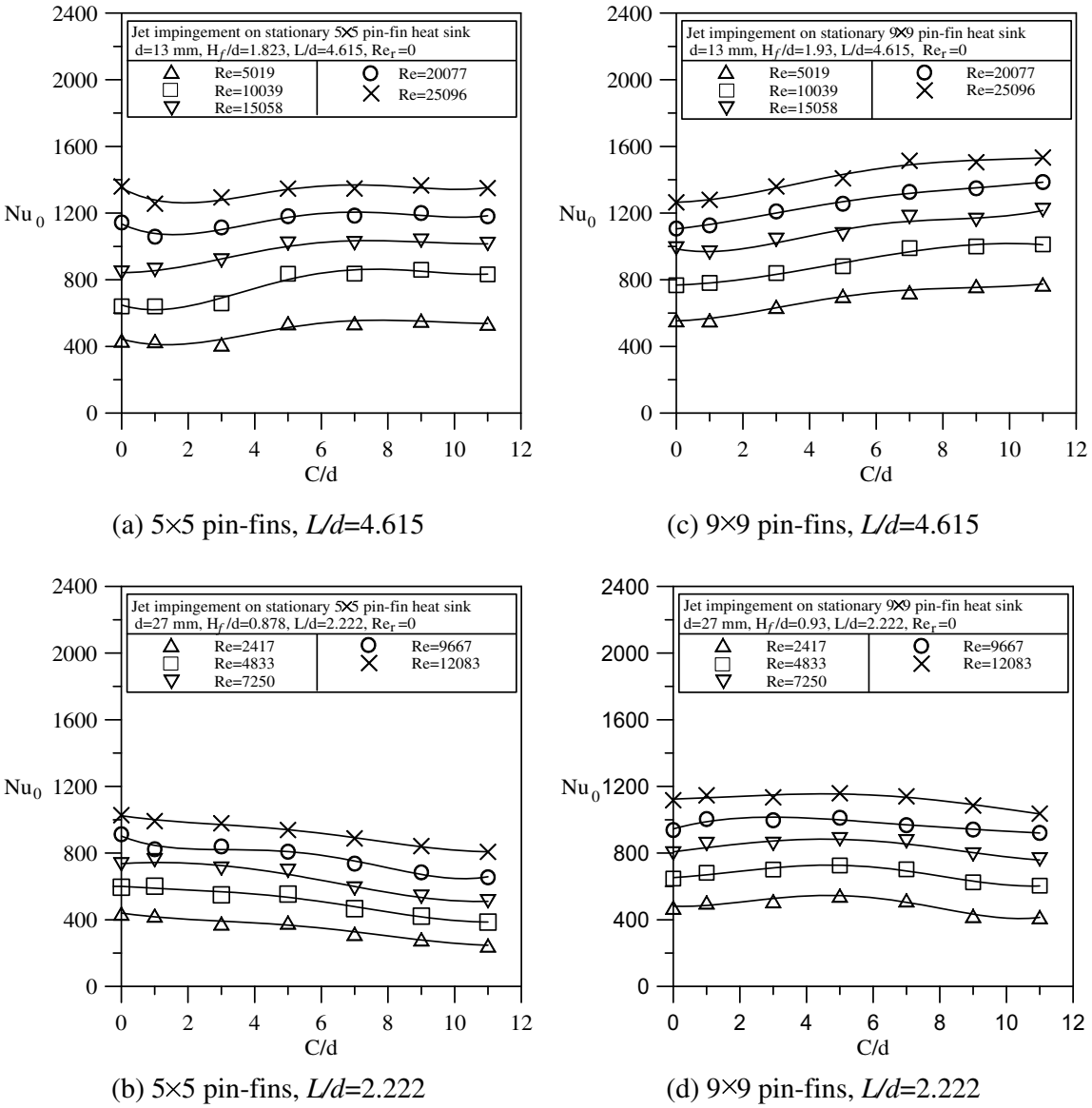

Fig. 5. Effects of C/d, L/d and Re on Nu_0 of a stationary heat sink with jet impingement.

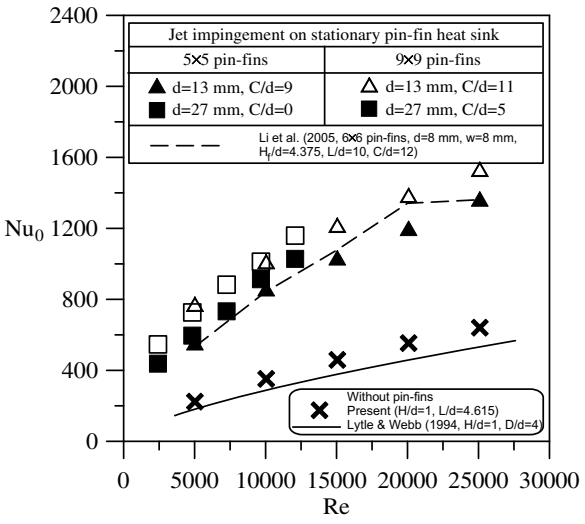

Fig. 6. Optimal parameters for maximum Nu_0 of a stationary heat sink with jet impingement.

stationary system with neither heat sink nor jet flow. At such condition, the total input heat flux (q_t) is divided into two parts: (1) the nature convective heat flux (q_{nc}) directly from the heated surface to the above air, and (2) the heat loss (q_{Loss}) from the heated surface to the ambience through the Bakelite disk.

$$q_{Loss} = q_t - q_{nc} = V \times I/A - h_{nc} \times (\overline{T_w} - T_a) \tag{5}$$

where h_{nc} is the heat transfer coefficient of the nature convection from the heated surface to the above air, and T_a is the ambient temperature. The empirical formula of h_{nc} is obtained from Ellison [29].

$$h_{nc} = 0.507 \times \left(\frac{\overline{T_w} - T_a}{P_{wet}}\right)^{0.25} \tag{6}$$

$$P_{wet} = \frac{L \times L}{2(L+L)} \tag{7}$$

In the heat-loss test, different values of q_t result in various $(\overline{T_w} - T_a)$. Using the results of the heat-loss test and Eqs. (5)–(7), the heat loss (q_{Loss}) as a function of $(\overline{T_w} - T_a)$ can be obtained. Also, the average Nusselt number (Nu) in Eq. (3) can be derived.

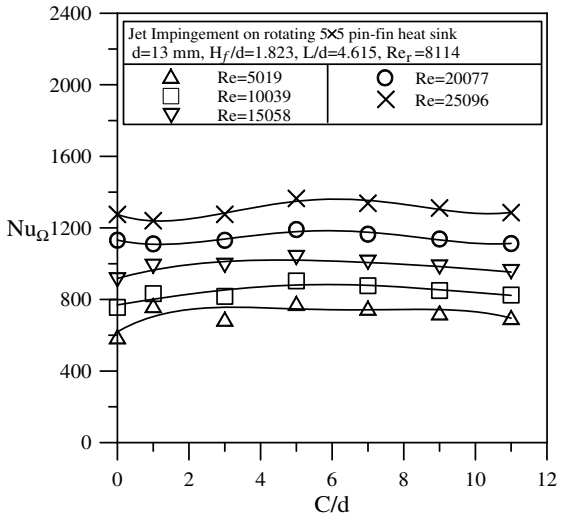

(a) 5· 5 pin-fins, L/d=4.615

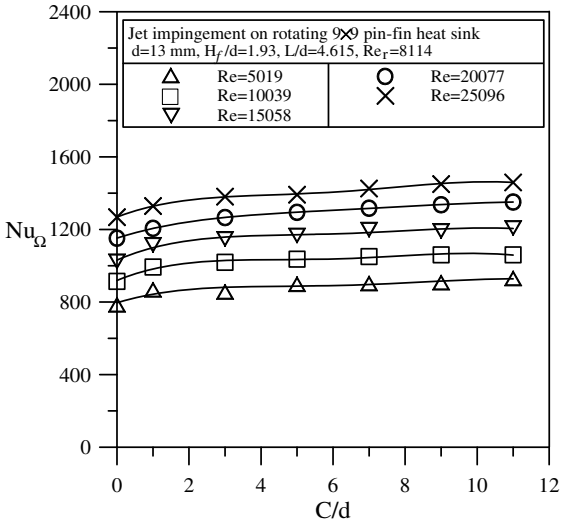

(c) 9· 9 pin-fins, L/d=4.615

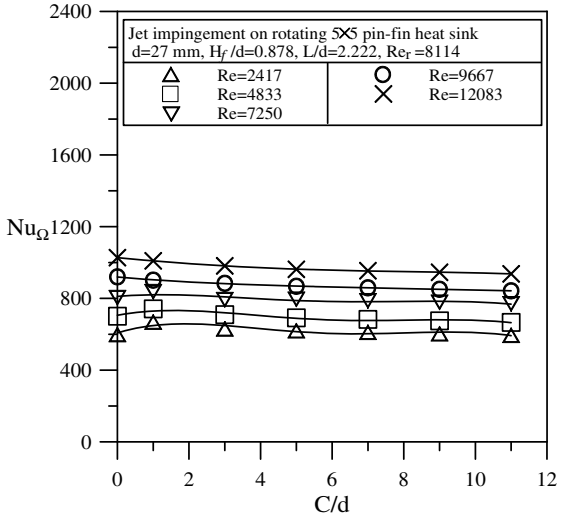

(b) 5· 5 pin-fins, L/d=2.222

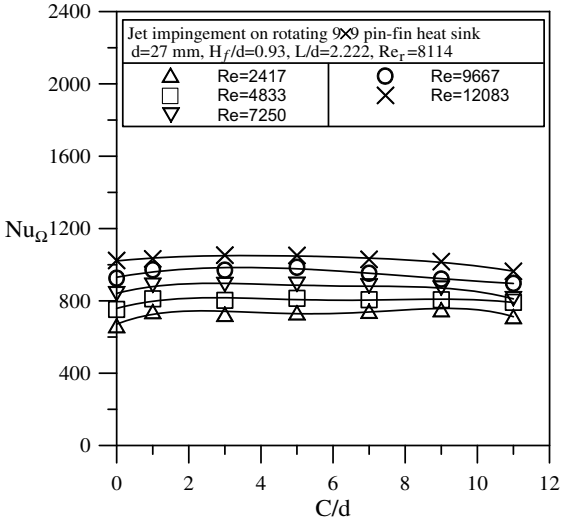

(d) 9· 9 pin-fins, L/d=2.222

Fig. 7. Effects of C/d, L/d and Re on Nu_Ω of a rotating heat sink with jet impingement.

The standard single-sample uncertainty analysis, as recommended by Kline and McClintock [30] and Moffat [31], is performed. Data supplied by the manufacturer of the instrumentation states that the measurement of flow velocity has a 1% error. The uncertainty in the measured temperature is ±0.2 °C. The experimental uncertainty in the convective heat flux (q_c) is estimated to be 3.4%. The experimental data herein reveal that the uncertainties in the jet Reynolds number (Re), the rotational Reynolds number (Re_r) and the average Nusselt number (Nu) are 2.0%, 2.3% and 7.6% at 95% confidence, respectively.

4. Results and discussion

In this section, the experimental results are discussed for the two heat sinks with respectively 5 × 5 and 9 × 9 square pin-fins. The overall cooling performances of the heat sinks are presented by the average Nusselt number (Nu) in terms of the relative length of the heat sink (L/d), the relative distance of nozzle-to-fin tip (C/d), the jet Reynolds numbers (Re) and the rotational Reynolds number (Re_r). The values of L/d are 4.615 and 2.222; C/d varies from 0 to 11; Re varies from 2417 to 25096; and Re_r varies from 0 to 8114.

Fig. 4 illustrates the flow visualization of the jet flow impinging onto a 9 × 9 pin-fin heat sink with L/d = 4.615 under stationary and rotational states. The incense is used as the trace of flow. In order to obtain the optimal images, small rotational rates (Re_r = 0, 638 and 1807) coupled with a fixed small jet-flow rate (Re = 1506) are employed. The images focus on the heat sink and the incense around it. It is found that, under the stationary condition as shown in Fig. 4(a)–(c), the jet flow impinges vertically onto the pin-fin heat sink, of which some jet flow pass-by from upper part of pin-fin heat sink and form vortices next to the jet, and some enter into the heat sink, turns an angle of 90 deg and then flows transversely outside of the heat sink from the passages between the pin-fins. Within the heat sink, the flow resistance is smaller due to shorter flow path along the centerline of the heat sink; but the flow resistance is bigger due to a longer flow path along the skew diagonal direction of the heat sink. Thus, air flow in the heat sink is mainly discharged along the centerline of the heat sink, which agrees with the 3-D simulation of similar flow field as discussed by Maveety and Jung [18]. Fig. 4(d)–(i) are the typical photos of incense flow at the rotating state. Comparing to those at the stationary state, the vortices next to the jet disappear. The jet flow is swaying above

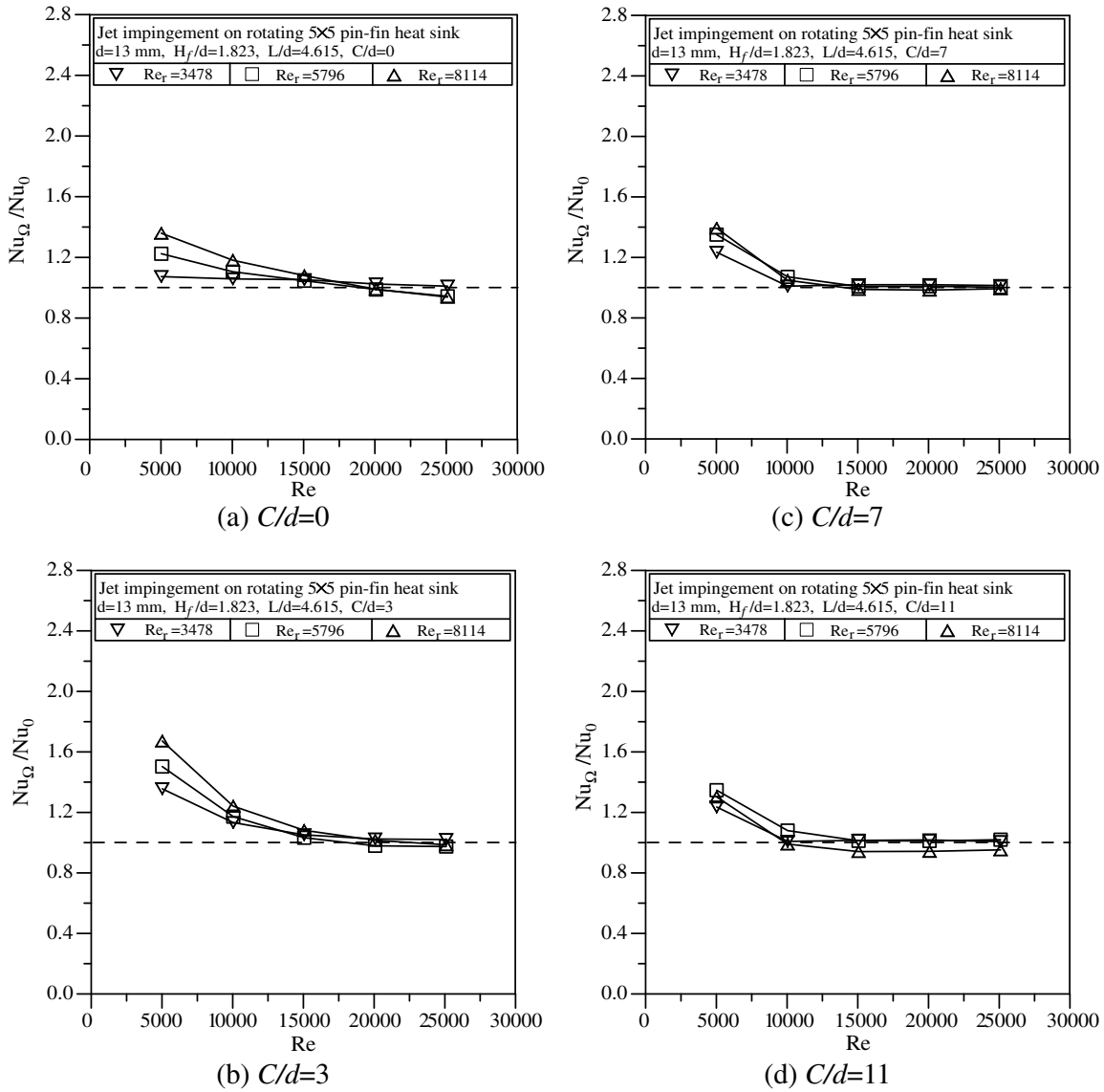

Fig. 8. Effect of Re_r on Nu_ω of a rotating 5 × 5 pin-fin heat sink with jet impingement (L/d = 4.615).

the rotating heat sink. Increasing the values of Re_r and C/d furthers the sway extent of the jet flow. In addition, Fig. 4(g) and (i) show little smoke appears at the lateral region of the rotating heat sink, demonstrating that increasing the rotational speed and impinging distance results in a lack of jet flow amount through the heat sink, which would go against the forced convection. However, the rotation of the heat sink still drives a peripheral flow, which promotes the heat transfer.

Fig. 5 discusses the effects of C/d, L/d and Re on average Nusselt number (Nu_0) of a stationary heat sink with jet impingement. It is found that, average Nusselt number (Nu_0) increases with increasing jet Reynolds number (Re), which is in-line with forced convection characteristics. If comparing average Nusselt numbers (Nu_0) under different L/d values, it is found that, in the event of same air flow rate rather than same jet Reynolds number (Re), average Nusselt number (Nu_0) of 5×5 pin-fin heat sink in $L/d = 4.615$ is 1.1–1.4 times of that in $L/d = 2.222$, and average Nusselt number (Nu_0) of 9×9 pin-fin heat sink in $L/d = 4.615$ is 1.2–2.0 times of that in $L/d = 2.222$. Thus, $L/d = 4.615$ presents better heat transfer performance. Additionally, average Nusselt number (Nu_0) of 9×9 pin-fin heat sink is about 1.2 times of 5×5 pin-fin heat sink in the case of $L/d = 4.615$, and 1.1 times in the case of $L/d = 2.222$, primarily owing to the fact that the extended surface area of 9×9 pin-fin heat sink is bigger than that of 5×5 pin-fin heat sink.

Fig. 5(a) also depicts that, for 5×5 pin-fin heat sink in the case of $L/d = 4.615$, the average Nusselt number (Nu_0) generally increases slightly with increasing C/d, apart from the case of $C/d = 0$. This is mainly because that the nozzle directly contacts the upper part of the pin-fin in the case of $C/d = 0$, so jet air can be completely guided into the pin-fin heat sink for improvement of forced convective heat transfer; the average Nusselt number (Nu_0) is bigger than that in the case of $C/d = 1$, since some air flow pass-by the heat sink from the upper spacing. However, average Nusselt number (Nu_0) increases when the value of C/d increases continuously ($C/d \geqslant 3$), and in the case of $C/d = 11$, it even becomes bigger than or equal to that in the case of $C/d = 0$. As illustrated in Fig. 4, most of jet flow will be rapidly discharged from the centerline of the heat sink, and a few discharged along the skew diagonal direction of the heat sink, so the surface area extended by pin-fins on the skew diagonal corners of the heat sink cannot be used

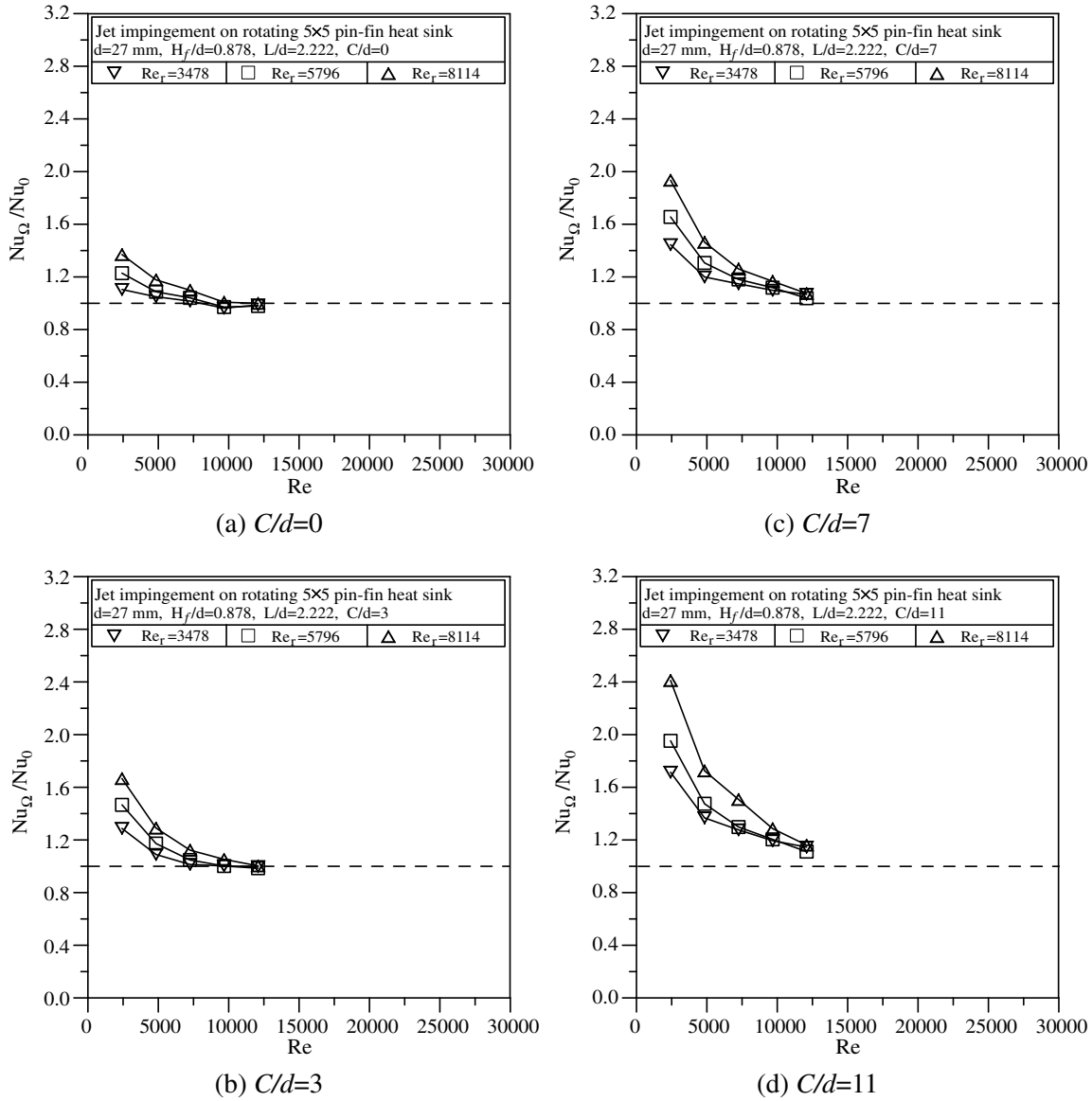

Fig. 9. Effect of Re_r on Nu_ω of a rotating 5×5 pin-fin heat sink with jet impingement ($L/d = 2.222$).

effectively for forced convective heat transfer. When the value of C/d increases continuously ($C/d \geqslant 3$), the jet projection zone of jet flow may expand although some air flow pass-by the heat sink from the upper spacing. In the case of $L/d = 4.615$, the expanded free jet projection zone will guide efficiently air flow into the heat sink, including the region of the skew diagonal corners of the heat sink, so the most surface area extended by pin-fins will be used effectively for heat transfer. Therefore, in the case of $L/d = 4.615$, average Nusselt number (Nu_0) in the event of $C/d = 11$ is even bigger than or equal to that in the event of $C/d = 0$, showing a similar trend for various jet Reynolds numbers (Re). Fig. 5(b) indicates that, for 5×5 pin-fin heat sink in $L/d = 2.222$, average Nusselt number (Nu_0) is highest in the case of $C/d = 0$, but may decline with the rise of C/d, owing to the fact that, when L/d is smaller (e.g. $L/d = 2.222$), the spread of jet increases and the expanded free jet projection zone may exceed the heat sink with increasing the C/d, accordingly the momentum of the jet flow decreases and the amount of air pass-by the heat sink will increase, consequently the heat transfer performance of the heat sink will reduce. This phenomenon occurs in the event of different jet Reynolds numbers (Re). Fig. 5(c) depicts the change of average Nusselt number (Nu_0) of 9×9pin-fin heat sink in the case of $L/d = 4.615$. The average Nusselt number (Nu_0) increases with increasing C/d. In addition, it is found from Fig. 5(d) that, for 9×9 pin-fin heat sink in $L/d = 2.222$ and $C/d \leqslant 5$, the average Nusselt number (Nu_0) rises slightly with C/d, but in the case of $C/d > 5$, the average Nusselt number (Nu_0) declines with C/d. As discussed above, a bigger amount of air flow will enter into the heat sink in the case of smaller C/d and bigger L/d, but cannot contact efficiently the pin-fins on the skew diagonal corners of the heat sink; a smaller amount of air flow will enter into the heat sink in the case of higher C/d and smaller L/d, but can contact efficiently all pin-fins. Therefore, the change of average Nusselt number (Nu_0) is attributable to the interaction of these factors.

Fig. 6 validates the present experimental test. Li et al. [20] used infrared thermography to measure the thermal performance of 6×6 pin-fin heat sinks with confined impinging air jet. By comparing the test samples of similar size, it is found that the distribution of average Nusselt numbers presented by Li et al. [20] is similar to that in this test. In addition, the results by Lytle and

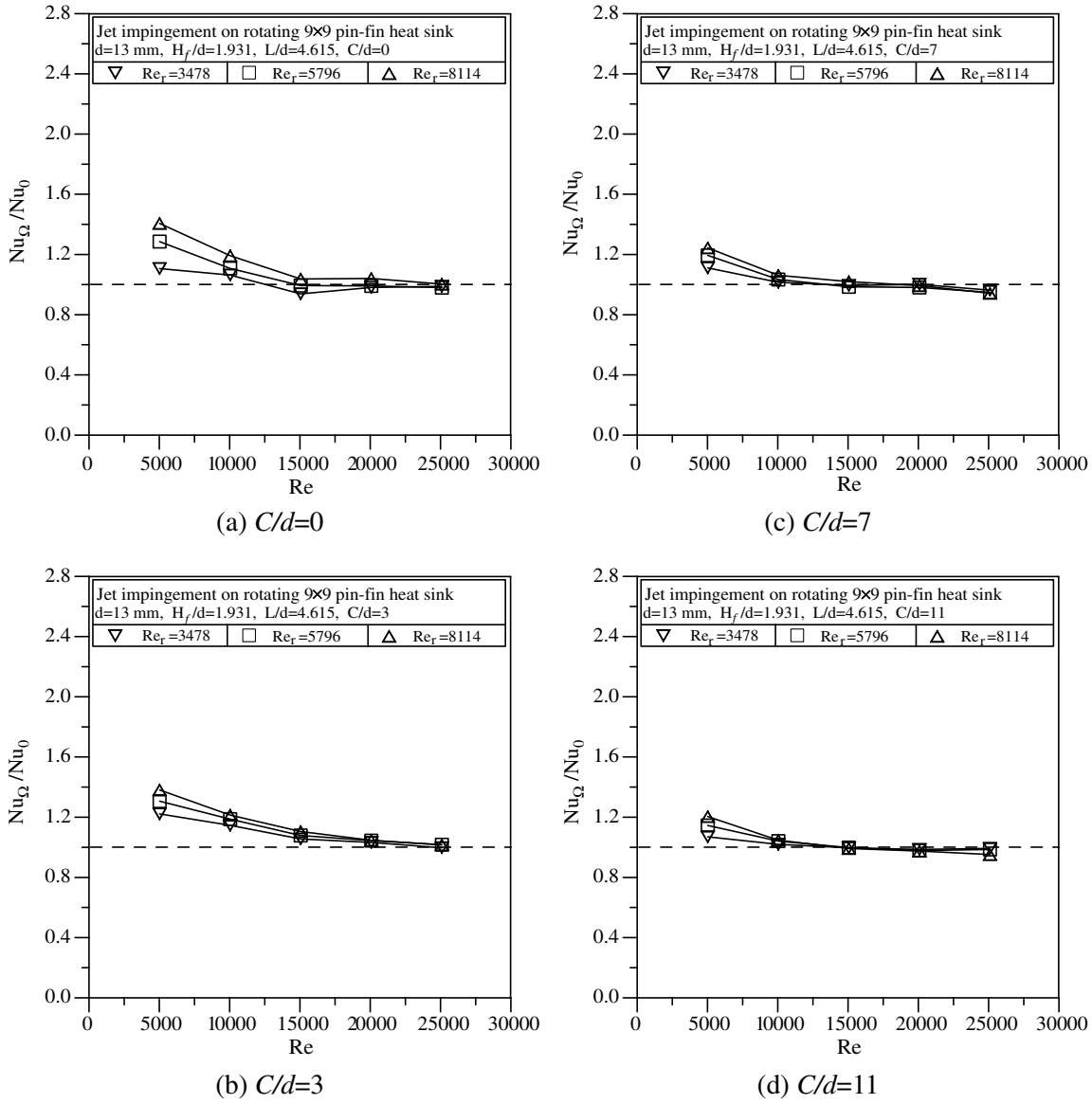

Fig. 10. Effect of Re_r on Nu_ω of a rotating 9×9 pin-fin heat sink with jet impingement ($L/d = 4.615$).

Webb [3] was also plotted in Fig. 5, wherein the present heat transfer data of a stationary plate with jet impingement was reasonably consistent with the predicted value of Lytle and Webb [3], in despite of some deviations arising from velocity profile, turbulence intensity, shape of target surface, etc., at the jet nozzle exit. If comparing the heat transfer with/without pin-fins, it could be seen that the heat transfer with pin-fins is 2–3 times without pin-fins, showing a considerable heat transfer enhancements for pin-fin heat sinks. Finally, Fig. 6 also discusses the optimum size parameters of stationary pin-fin heat sink under impinging jet flow in the case of maximum average Nusselt number (Nu_0). It is found that, in the event of same air flow rate (rather than same jet Reynolds number), the 9×9 pin-fin heat sink with $L/d = 4.615$ and $C/d = 11$ has the maximum average Nusselt number (Nu_0).

According to the measured data and also the effects of relevant parameters on average Nusselt number (Nu_0) as discussed above, the empirical formulas of average Nusselt number (Nu_0) in terms of C/d and Re are derived separately for 5×5 and 9×9 pin-fin heat sinks under different L/d values.For 5×5 pin-fin heat sink:

$$Nu_0 = [3.027 - 0.00555(C/d - 11.737)^2]Re^{0.611} \quad \text{for } L/d = 4.615 \tag{8}$$

$$Nu_0 = [4.013 - 0.00532(C/d + 6.620)^2]Re^{0.598} \quad \text{for } L/d = 2.222 \tag{9}$$

For 9×9 pin-fin heat sink:

$$Nu_0 = [15.444 - 0.01465(C/d - 17.683)^2]Re^{0.460} \quad \text{for } L/d = 4.615 \tag{10}$$

$$Nu_0 = [9.477 - 0.05028(C/d - 4.204)^2]Re^{0.516} \quad \text{for } L/d = 2.222 \tag{11}$$

The average deviation between the predicted results by Eqs. (8)–(11) and the experimental data is within ±5%, of which the biggest deviation (within ±15%) occurs at the case of 5×5 pin-fin heat sink with $L/d = 4.615$, $C/d = 0$ and $Re = 12083$.

In Fig. 7, the conditions of $Re_r = 8114$ are taken as typical cases, the effects of C/d, L/d and Re on average Nusselt number (Nu_Ω) of a rotating heat sink with jet impingement are discussed. It is found that, average Nusselt number (Nu_Ω) increases slightly with C/d in

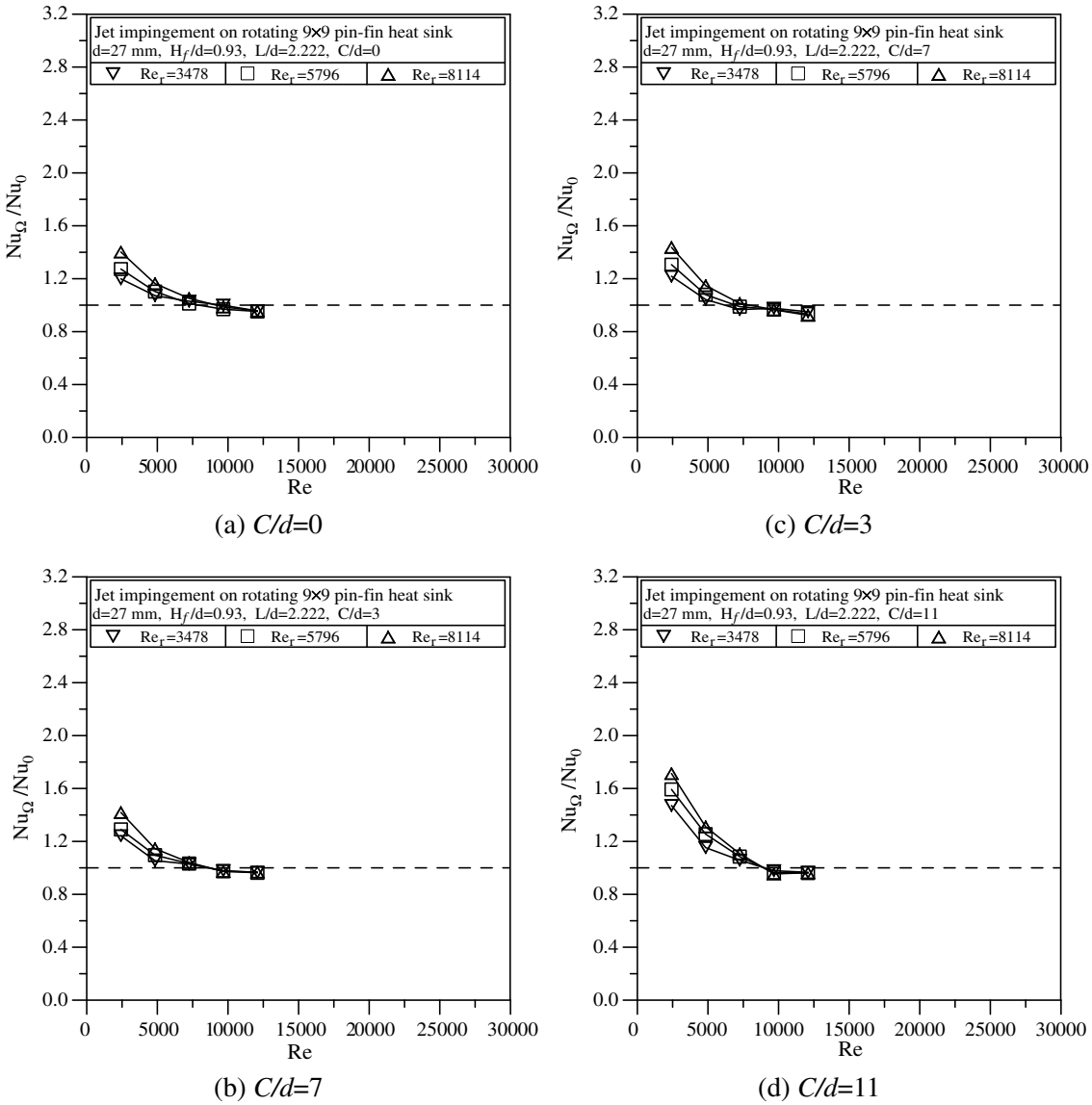

Fig. 11. Effect of Re_r on Nu_Ω of a rotating 9×9 pin-fin heat sink with jet impingement ($L/d = 2.222$).

the case of L/d = 4.615, but it drops slightly with rise of C/d in the case of L/d = 2.222. This tendency generally is similar to that in stationary state. However, some results in rotational state differ from those in stationary state. Firstly, in the case of $Re \leqslant 15058$ under rotational state, average Nusselt number (Nu_Ω) in the event of C/d = 0 is obviously smaller than that in the event of C/d = 1, contrary to the cases in stationary state; secondly, when Re becomes smaller, average Nusselt number (Nu_Ω) will increase significantly due to the rotational effect, otherwise remains unchanged. The above mention demonstrates that, the rotational effect really affects the heat transfer of present impinging-cooling system. In the occurrence of rotation, the impinging flow field may change within and outside the heat sink. Within the heat sink, pin-fin and air flow will generate a relative speed in the peripheral direction, which becomes bigger if located far away from the center of the rotation axle. It is helpful to heat transfer. Outside the heat sink, the flow field around and over the heat sink may yield extra disturbance due to the influence of rotating heat sink, which may also improve the heat transfer performance of heat sink. Yet, when the Re is relatively big, the effect of rotation on heat transfer enhancement becomes unobvious, showing that the cooling is mainly dominated by forced convection of jet flow.

Figs. 8–11 present the effect of rotational Reynolds number (Re_r) on average Nusselt number (Nu_Ω) for various Re, L/d and C/d. The relationship between Nu_Ω/Nu_0 and Re was plotted. The results demonstrate that a bigger Re_r meant a more obvious heat transfer enhancement in the case of smaller Re, but the heat transfer enhancement by rotation decreased with increasing Re. For some cases with larger Re, the rotation even impaired the heat transfer. The reason can be explained as follows. When the pin-fin heat sink is rotating, the inside air generates the peripheral velocity related to the pin-fins, promoting heat transfer. On the other hand, the rotating heat sink stops the jet flow from going across the pin-fins and reaching the heated spreader, reducing the heat transfer by the jet impingement. Therefore, if the heat transfer enhancement by rotation can not compensate for the heat transfer reduction by rotation, the average Nusselt number at rotational state will less than that at stationary state (i.e. $Nu_\Omega/Nu_0 < 1$). Generally, as L/d is smaller and

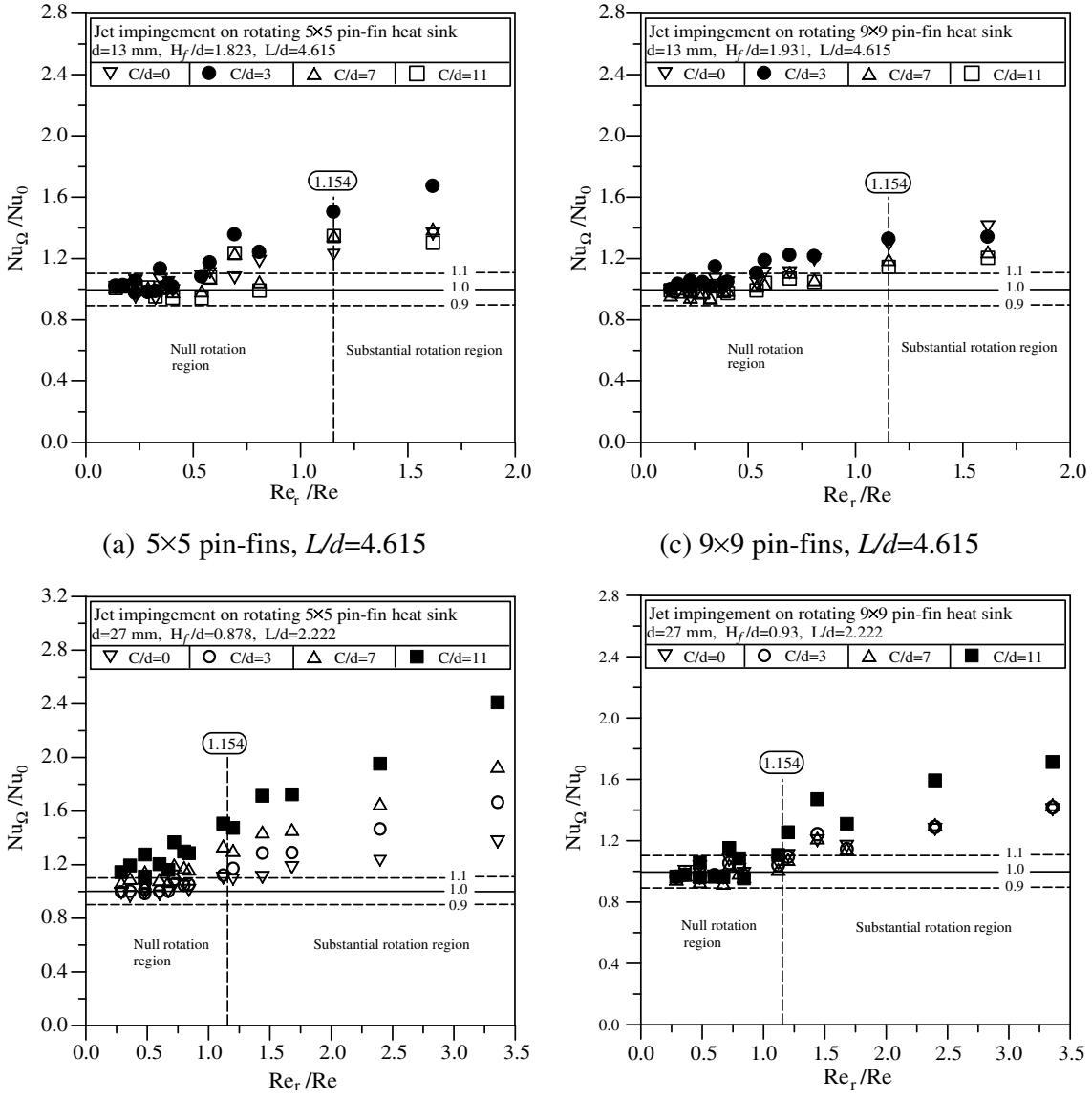

Fig. 12. Nu_Ω/Nu_0 as a function of Re_r/Re.

C/d is bigger, the jet air in the vicinity of outer perimeter of the jet nozzle easily bypass the pin-fin heat sink. Less air inside heat sink results less impaired effect on impinging-cooling performance by rotation. Furthermore, the rotation also perturbs the bypass air flow around the heat sink to promote the heat transfer. So the effect of rotation on the heat transfer enhancement will more obvious at adequately small L/d and appropriately big C/d. In this work, the heat transfer enhancement of system from rotational effect in $L/d = 2.222$ is higher than in $L/d = 4.615$; among the systems in $L/d = 2.222$, bigger rotational heat transfer enhancement (Nu_Ω/Nu_0) exists in the case of $C/d = 9$–11, but among the systems in $L/d = 4.615$, bigger rotational heat transfer enhancement (Nu_Ω/Nu_0) exists in the case of $C/d = 1$–3.

In principle, heat transfer enhancement increases with Re_r. However, the heat transfer varied little with Re increases, possibly because two forced convections apply – one associated with jet impingement, and the other associated with rotation. When Re is sufficiently large in relation to Re_r, the forced convection associated with jet impingement dominates the cooling performance and that associated with rotation is negligible. Therefore, a dimensionless parameter, Re_r/Re, can be utilized to identify whether the rotation is substantial. Fig. 12 plots Nu_Ω/Nu_0 as a function of Re_r/Re. Considering the experimental uncertainty yields a value of Nu_Ω/Nu_0 of larger than 1.1 as the effective factor of heat transfer enhancement. Given $Nu_\Omega/Nu_0 \geqslant 1.1$, the experimental results indicate that the rotations are substantial at $Re_r/Re \geqslant 1.154$ for the present study.

5. Summary and conclusion

Experimental investigation of heat transfer enhancement of jet impingement onto the rotating pin-fin heat sink is completed. Air is used as impinging coolant, while the 5×5 and 9×9 pin-fin heat sinks with uniformly in-line arrangement are employed. Variable parameters are the relative length of the heat sink (L/d), the relative distance of nozzle-to-fin tip (C/d), the jet Reynolds number (Re) and the rotational Reynolds number (Re_r). The following conclusions are drawn.

(1) The flow characteristics of the jet flow impinging onto a pin-fin heat sink under stationary and rotational states are investigated successfully by the smoke visualization.

(2) The effects of C/d, L/d and Re on average Nusselt number (Nu_0) of a stationary heat sink with jet impingement are discussed. It is found that Nu_0 increases with Re. Based on the same air flow rate, Nu_0 of 5×5 pin-fin heat sink in $L/d = 4.615$ is 1.1–1.4 times of that in $L/d = 2.222$, and Nu_0 of 9×9 pin-fin heat sink in $L/d = 4.615$ is 1.2–2.0 times of that in $L/d = 2.222$. Additionally, Nu_0 of 9×9 pin-fin heat sink is about 1.2 times of 5×5 pin-fin heat sink in the case of $L/d = 4.615$, and 1.1 times in the case of $L/d = 2.222$. Furthermore, the parameter C/d results in various influences on Nu_0 for the 5×5 and 9×9 pin-fin heat sinks with various L/d. Finally, the empirical formulas of Nu_0 in terms of C/d and Re are derived separately for 5×5 and 9×9 pin-fin heat sinks with different L/d values.

(3) The effect of Re_r on average Nusselt number (Nu_Ω) of a rotating heat sink with jet impingement is investigated, which generally is similar to that in stationary state. The results demonstrate that a bigger Re_r meant a more obvious heat transfer enhancement (Nu_Ω/Nu_0) in the case of smaller Re, but Nu_Ω/Nu_0 decreased with increasing Re. In this work, Nu_Ω/Nu_0 in $L/d = 2.222$ is higher than in $L/d = 4.615$; among the systems in $L/d = 2.222$, bigger Nu_Ω/Nu_0 exists in the case of $C/d = 9$–11, but among the systems in $L/d = 4.615$, bigger Nu_Ω/Nu_0 exists in the case of $C/d = 1$–3.

(4) Considering the experimental uncertainty yields a value of Nu_Ω/Nu_0 of larger than 1.1 as the effective factor of heat transfer enhancement. Given $Nu_\Omega/Nu_0 \geqslant 1.1$, the results indicate that the rotations are substantial at $Re_r/Re \geqslant 1.154$ for the present study.

Acknowledgements

The authors thank the National Science Council of the Republic of China for financially supporting this research under Contract Nos. NSC-97-2221-E-344-003 and NSC-97-2221-E-270-006.

References

[1] K. Jambunathan, E. Lai, M.A. Moss, B.L. Button, A review of heat transfer data for single circular jet impingement, Int. J. Heat Fluid Flow 13 (2) (1992) 106–115.
[2] D.J. Womac, S. Ramadhyani, F.P. Incropera, Correlating equations for impingement cooling of small heat sources with single circular liquid jets, ASME J. Heat Transfer 115 (1993) 106–115.
[3] D. Lytle, B.W. Webb, Air jet impingement heat transfer at low nozzle-plate spacings, Int. J. Heat Mass Transfer 37 (12) (1994) 1687–1697.
[4] J.Y. San, C.H. Huang, M.H. Shu, Impingement cooling of a confined circular air jet, Int. J. Heat Mass Transfer 40 (6) (1997) 1355–1364.
[5] M. Behnia, S. Parneix, Y. Shabany, P.A. Durbin, Numerical study of turbulent heat transfer in confined and unconfined impinging jets, Int. J. Heat Fluid Flow 20 (1999) 1–9.
[6] A.H. Beitelmal, M.A. Saad, C.D. Patel, Effects of surface roughness on the average heat transfer of an impinging air jet, Int. Commun. Heat Mass Transfer 27 (1) (2000) 1–12.
[7] S. Sathe, K.M. Kelkar, K.C. Karki, C. Lamb, S.V. Patankar, Numerical predication of flow and heat transfer in an impingement heat sink, ASME J. Electron. Pack. 119 (1997) 58–63.
[8] E.M. Sparrow, E.D. Larson, Heat transfer from pin-fins situated in an oncoming longitudinal flow which turns to crossflow, Int. J. Heat Mass Transfer 25 (5) (1982) 603–613.
[9] E.D. Larson, E.M. Sparrow, Performance comparisons among geometrically different pin-fin arrays situated in an oncoming longitudinal flow, Int. J. Heat Mass Transfer 25 (5) (1982) 723–725.
[10] E.M. Sparrow, A.P. Suopys, M.A. Ansari, Effect of inlet, exit, and fin geometry on pin fins situated in a turning flow, Int. J. Heat Mass Transfer 27 (7) (1984) 1039–1054.
[11] L.G. Hansen, B.W. Webb, Air jet impingement heat transfer from modified surfaces, Int. J. Heat Mass Transfer 36 (4) (1993) 989–997.
[12] G. Ledezma, A.M. Morega, A. Bejan, Optimal spacing between pin fins with impinging flow, ASME J. Heat Transfer 118 (1996) 570–577.
[13] L.A. Brignoni, S.V. Garimella, Experimental optimization of confined air jet impingement on a pin fin heat sink, IEEE Trans. Compon. Pack. Technol. 22 (3) (1999) 399–404.
[14] Y. Kondo, M. Behnia, W. Nakayama, H. Matsushima, Optimization of finned heat sinks for impingement cooling of electronic packages, ASME J. Electron. Pack. 120 (1998) 259–266.
[15] Y. Kondo, H. Matsushima, T. Komatsu, Optimization of pin-fin heat sinks for impingement cooling of electronic packages, ASME J. Electron. Pack. 122 (2000) 240–246.
[16] J.G. Maveety, J.F. Hendricks, A heat sink performance study considering material, geometry, nozzle placement, and Reynolds number with air impingement, ASME J. Electron. Pack. 121 (1999) 156–161.
[17] J.G. Maveety, H.H. Jung, Design of an optimal pin-fin heat sink with air impingement cooling, Int. Commun. Heat Mass Transfer 27 (2) (2000) 229–239.
[18] J.G. Maveety, H.H. Jung, Heat transfer from square pin-fin heat sinks using air impingement cooling, IEEE Trans. Compon. Pack. Technol. 25 (3) (2002) 459–469.
[19] H.A. El-Sheikh, S.V. Garimella, Enhancement of air impingement heat transfer using pin-fin heat sinks, IEEE Trans. Compon. Pack. Technol. 23 (2) (2000) 300–328.
[20] H.Y. Li, S.M. Chao, G.L. Tsai, Thermal performance measurement of heat sinks with confined impinging jet by infrared thermography, Int. J. Heat Mass Transfer 48 (2005) 5386–5394.
[21] H.Y. Li, K.Y. Chen, Thermal performance of plate-fin heat sinks under confined impinging jet conditions, Int. J. Heat Mass Transfer 50 (2007) 1963–1970.
[22] J.S. Issa, A. Ortega, Experimental measurements of the flow and heat transfer of a square jet impinging on an array of square pin fins, ASME J. Electron. Pack. 128 (2006) 61–70.
[23] T.W. Lin, M.C. Wu, L.K. Liu, C.J. Fang, Y.H. Hung, Cooling performance of using a confined slot jet impinging onto heated heat sinks, ASME J. Electron. Pack. 128 (2006) 82–91.

[24] M. Itoh, M. Okada, An experimental study of the radial wall jet on a rotating disk, Exp. Therm. Fluid Sci. 17 (1998) 49–56.
[25] Y.R. Shieh, C.J. Li, Y.H. Hung, Heat transfer from a horizontal wafer-based disk of multi-chip modules, Int. J. Heat Mass Transfer 42 (1999) 1007–1022.
[26] M.M. Rahman, Analysis of simultaneous gas absorption and chemical reaction to a thin liquid film over a spinning disk, Int. Commun. Heat Mass Transfer 27 (2000) 303–314.
[27] Y. Minagawa, S. Obi, Development of turbulent impinging jet on a rotating disk, Int. J. Heat Fluid Flow 25 (2004) 759–766.
[28] T.M. Jeng, S.C. Tzeng, D.C. Liu, Heat transfer behavior in a rotating aluminum foam heat sink with a circular impinging jet, Int. J. Heat Mass Transfer 51 (2008) 1205–1215.
[29] G.N. Ellison, Thermal Computations for Electronic Equipment, Van Nostrand Reinhold Company, New York, 1984. pp. 29–45.
[30] S.J. Kline, F.A. Mcclintock, Describing uncertainties in single-sample experiments, Mech. Eng. (1953) 3–8.
[31] R.J. Moffat, Contributions to the theory of single-sample uncertainty analysis, ASME J. Fluids Eng. 104 (1986) 250–260.